Dynamic response of graphene to thermal impulse

Jingchao Zhang,[1] Xiaopeng Huang,[1] Yanan Yue,[1] Jianmei Wang,[2] and Xinwei Wang[1,3,*]

[1]*2010 Black Engineering Building, Department of Mechanical Engineering, Iowa State University, Ames, Iowa 50011, USA*

[2]*Department of Energy and Power Engineering, Wuhan University, Wuhan 430072, People's Republic of China*

[3]*School of Environmental and Municipal Engineering, Qingdao Technological University, Qingdao 266033, People's Republic of China*

(Received 22 September 2011; revised manuscript received 8 November 2011; published 1 December 2011)

A transient molecular dynamics technique is developed to characterize the thermophysical properties of two-dimensional graphene nanoribbons (GNRs). By directly tracking the thermal-relaxation history of a GNR that is heated by a thermal impulse, we are able to determine its thermal diffusivity quickly and accurately. We study the dynamic thermal conductivity of various length GNRs of 1.99 nm width. Quantum correction is applied in all of the temperature calculations and is found to have a critical role in the thermal-transport study of graphene. The calculated specific heat of GNRs agrees well with that of graphite at 300.6 and 692.3 K, showing little effect of the unique graphene structure on its ability to store thermal energy. A strong size effect on GNR's thermal conductivity is observed and its theoretical values for an infinite-length limit are evaluated by data fitting and extrapolation. With infinite length, the 1.99-nm-wide GNR has a thermal conductivity of 149 W m^{-1} K^{-1} at 692.3 K, and 317 W m^{-1} K^{-1} at 300.6 K. Our study of the temperature distribution and evolution suggests that diffusive transport is dominant in the studied GNRs. Non-Fourier heat conduction is observed at the beginning of the thermal-relaxation procedure. Thermal waves in GNR's in-plane direction are observed only for phonons in the flexural direction (ZA mode). The observed propagation speed ($c = 4.6$ km s^{-1}) of the thermal wave follows the relation of $c = v_g/\sqrt{2}$ (v_g is the ZA phonon group velocity). Our thermal-wave study reveals that in graphene, the ZA phonons transfer thermal energy much faster than longitudinal (LA) and transverse (TA) modes. Also, ZA↔ZA energy transfer is much faster than the ZA↔LA/TA phonon energy transfer.

DOI: 10.1103/PhysRevB.84.235416 PACS number(s): 65.80.Ck, 66.30.Xj, 66.70.−f, 63.20.−e

I. INTRODUCTION

Graphene is a monolayer of graphite arranged in a honeycomb lattice of sp^2 bonded carbon atoms[1] and it has attracted much attention over the past decade due to its extraordinary electronic and thermal properties.[2–5] Graphene nanoribbon (GNR), which is a narrow strip (typically <20 nm) of graphene, also became the subject of significant research because of its extraordinary electrical, thermal, and mechanical properties with significant application potential in future nanoelectronic and mechanical devices. These distinguishing properties of GNRs, which indicate that GNRs are a promising material for nanoeletronic applications, have been extensively studied both theoretically and experimentally.[2,6–9] Owing to the edge effect and quantum confinement, GNRs are expected to exhibit outstanding thermal properties.[10]

Both experimental and numerical methods have been conducted to study the thermal properties of GNR, and ultrahigh thermal conductivity has been observed.[11,12] Recent measurements of the thermal conductivity (k) of a partially suspended graphene sheet revealed a thermal conductivity as high as 5300 W m^{-1} K^{-1} at room temperature (RT).[11] Other experiments[12] suggest that graphene has thermal conductivity of 3000−5000 W m^{-1} K^{-1} for a length l of ∼10 μm. This high thermal conductivity exceeds that of graphite and is partly attributed to the long phonon mean free path (MFP) in carbon nanostructures. Several research groups,[10,13] using the Brenner potential and nonequilibrium molecular dynamics (NEMD) simulations, found much lower values of k in the order of several hundreds of W m^{-1} K^{-1} depending on the width, edge type (armchair or zigzag), and roughness. First-principles calculations by Nika *et al.*[14] and Kong *et al.*[15] obtained k values of graphene in the range of 2000−6000 W m^{-1} K^{-1}. In several previous MD simulation investigations, however, the results turned out to be contradictory to that study. Hu *et al.*[16] calculated the thermal conductivity of GNRs (up to ∼4 nm wide and ∼10 nm long) around 2000 W m^{-1} K^{-1}. The size of the GNRs explored by Hu *et al.* is much smaller than graphene's phonon mean free path (MFP), which is about 775 nm at RT.[12] Therefore, the thermal-conductivity result in Hu's work is much higher than expected since the value is beyond the upper ballistic bounds.[17] It has been pointed out that quantum ballistic transport could not be fully described by MD simulation, and violation of the ballistic upper bounds may be observed when calculating thermal conductance.[18] Although the thermal properties of GNRs have been studied using various approaches, the length effect has not been investigated yet and the size effect has not been well understood. Moreover, almost all previous numerical methods are based on a steady-state temperature gradient to calculate the static thermal conductivity. The dynamic response of graphene to thermal impulses has not been explored in the past.

In this work, MD simulation is performed to study the dynamic response of GNR to thermal impulse based on the second generation of the Brenner potential.[19] A transient technique is developed to numerically measure the thermal diffusivity of GNR based on its thermal response. This technique features a comparably fast MD-simulation implementation and low data uncertainty. To study the size effect on the dynamic thermal conductivity of GNR, different lengths (from 14.9 to 999.9 nm) of GNR structures with 1.99 nm width are used. Quantum correction is applied to both GNR's thermal-conductivity (k) and specific-heat (c_p) calculation. In Sec. II, we first introduce the pulsed

laser-assisted thermal relaxation (PLTR) technique, from which our numerical method is derived. Details of this numerical method are then discussed with its application to numerically measure GNR's dynamic thermal conductivity. Section III provides MD-simulation results and our analysis of the size effect on GNR's thermal conductivity. Non-Fourier heat conduction is analyzed in detail and thermal-wave propagation in GNR's in-plane direction is studied.

II. PHYSICS OF THE DYNAMIC RESPONSE

In MD simulations, to determine the thermal conductivity of materials, nonequilibrium and equilibrium techniques can be applied. Traditional numerical methods such as NEMD simulations employ heat sources and sinks to generate the temperature gradient for thermal-conductivity calculations. Based on Fourier's law of heat conduction, the thermal conductivity can be calculated from the temperature gradient and heat flux. An alternative approach to determine the thermal conductivity is equilibrium molecular dynamic (EMD) simulations based on the Green-Kubo expression that relates k to the integral over time t of the heat-flux autocorrelation function by

$$\lambda = \frac{1}{3Vk_BT^2}\int_0^\infty \langle J(t)\cdot J(0)\rangle dt, \qquad (1)$$

where k_B is the Boltzmann constant, V is the volume, T is the temperature of the sample, and the angular brackets denote an ensemble average. The thermal conductivity can be calculated using Eq. (1) once the heat-flux vector $J(t)$ is known. A detailed comparison of the MD techniques for computing thermal conductivity was conducted by Schelling *et al.*[20] Generally speaking, the NEMD approach requires large temperature gradients, which takes relatively long simulation times and has significant boundary-condition issues at the interfaces. The results calculated using the EMD method depend sensitively on the initial conditions of each simulation, thus necessitating a large ensemble of simulations. The slow convergence of the autocorrelation function further increases the computational demand, requiring long integration time periods.[21] Therefore, in the present study, a transient cooling method is developed to evaluate the dynamic thermal conductivity of GNR with a much shorter computational time requirement, while bearing a higher level of accuracy.[22]

A. Dynamic method and mathematical model

The numerical method used in our MD simulation process is derived from the PLTR technique, which is developed by our group to measure the thermal diffusivity of one-dimensional micro/nanoscale structures in experiment.[22,23] In the PLTR technique, the to-be-measured sample is suspended over two copper electrodes. When running the experiment, a nanosecond laser pulse is used to irradiate the sample wire uniformly to induce a temperature increase (ΔT). The configuration of this experiment is shown in Fig. 1(a). Right after the pulsed laser heating, the temperature of the sample will gradually go down. The temperature evolution of the

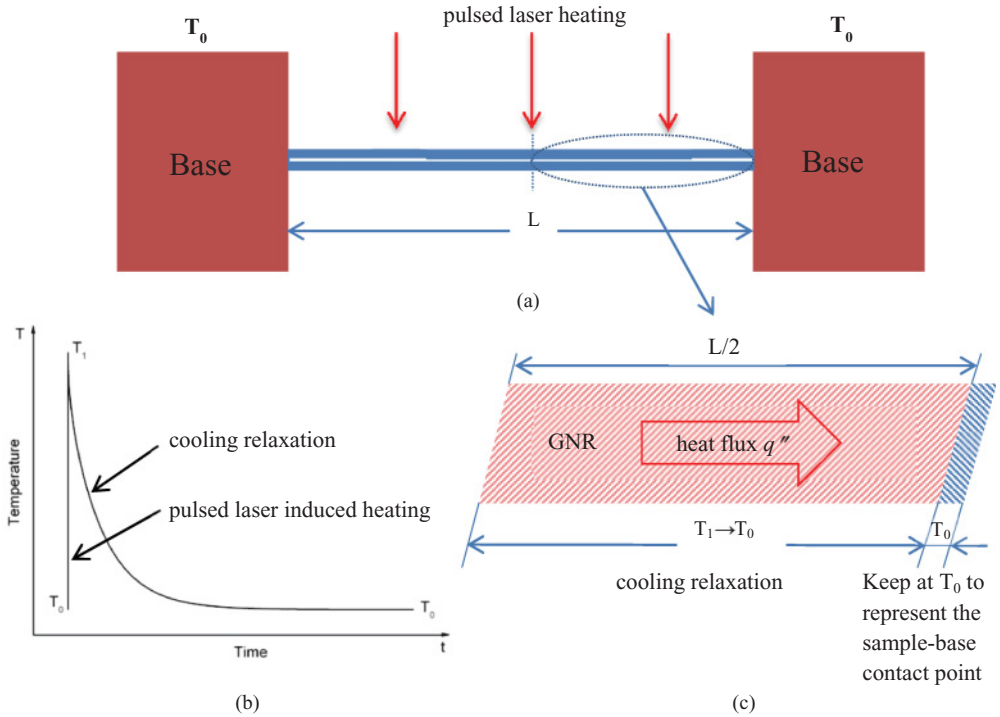

FIG. 1. (Color online) Schematic of experiment and MD simulation methods for PLTR. (a) A sample is suspended over two electrodes in experiment. The temperature of the two bases is kept at T_0 (RT). (b) Changes of sample temperature after pulsed laser heating. The sample temperature is T_0 at the initial state, and then rises to T_1 quickly because of the induced heating by the laser pulse. Cooling relaxation continues until the sample's temperature reaches T_0 again. (c) Numerical principles derived from the PLTR technique. The temperature of the system is set at T_1 initially. Then, one end of the GNR is kept at a low temperature (T_0) to represent the sample-base contact point.

sample is shown in Fig. 1(b). Such temperature relaxation is strongly determined by the samples' thermal diffusivity and length. From this temperature-relaxation history, the thermal diffusivity of the wire can be determined with sound accuracy. In experiment, the length of the wire is significantly greater than its diameter, which will simplify the physical model to one dimensional (1D). The thermal conductivity is determined via the 1D heat-transfer equation

$$\frac{\partial \rho c_p T}{\partial t} = k\frac{\partial^2 T}{\partial x^2} + \dot{q}, \tag{2}$$

with homogeneous boundary conditions and initial conditions, $T(x = 0, t) = T(x = L, t) = 0$ and $T(x, t = 0) = 0$. Here, T only represents the temperature variation induced by the thermal impulse and $\dot{q}$ represents the rate of thermal-energy generation induced by the laser pulse (pulse width Δt) heating. The solution to the partial differential equation described by Eq. (2) can be obtained from the integral of the Green's function,

$$G_{X11}(x,t|x',\tau) = \frac{2}{L}\sum_{m=1}^{\infty} \exp[-m^2\pi^2\alpha(t-\tau)/L^2] \times \sin\left(m\pi\frac{x}{L}\right)\sin\left(m\pi\frac{x'}{L}\right). \tag{3}$$

The average temperature of the wire $T(t)$ for $0 < t \leqslant \Delta t$ is expressed as

$$T(t) = \frac{1}{L}\int_{x=0}^{L} T(x,t)dx = \frac{8\dot{q}L^2}{k\pi^4}\sum_{m=1}^{\infty}\frac{1-\exp[-(2m-1)^2\pi^2\alpha t/L^2]}{(2m-1)^4}. \tag{4}$$

For time t larger than Δt, we have

$$T(t) = \frac{8\dot{q}L^2}{k\pi^4}\sum_{m=1}^{\infty}\frac{\exp[-(2m-1)^2\pi^2\alpha t/L^2]\{\exp[(2m-1)^2\pi^2\alpha\Delta t/L^2]-1\}}{(2m-1)^4}. \tag{5}$$

After normalizing as $T^* = [T(t) - T_{\min}]/(T_{\max} - T_{\min})$ ($T_{\min}$ is 0 and $T_{\max}$ is the maximum temperature increase of the sample calculated as $\dot{q}\Delta t/\rho c_p$), and using the relation $k = \rho c_p \alpha$, where ρ is mass density, c_p is the specific heat, and α is the thermal diffusivity, the normalized temperature relaxation simplified using Taylor expansions can be written as

$$T^* = \frac{8}{\pi^2}\sum_{m=1}^{\infty}\frac{\exp[-(2m-1)^2\pi^2\alpha t/L^2]}{(2m-1)^2}. \tag{6}$$

Equation (6) shows that for any kind of material of arbitrary length, the normalized temperature relaxation follows the same shape with respect to the Fourier number, $F_o(= \alpha t/L^2)$.[22,23] Further convergence study shows that to make the summation in Eq. (6) converge, the value of the term related to m should be less than 10^{-3} of the summation from terms 1 to $m - 1$. When $m = 15$, the summation in Eq. (6) will converge to a stable value with negligible error. The thermal diffusivity of the sample is determined by global data fitting of the temperature-relaxation curve. In this method, the normalized temperature decrease is calculated using Eq. (6) by using different trial values of thermal diffusivity. The trial value giving the best fit (least squares) of the experimental data is taken as the sample's thermal diffusivity.

B. Atomic potential and MD domain construction

In our MD simulation, the second-generation Brenner potential,[19] i.e., reactive empirical bond-order (REBO), based on the Tersoff potential[24,25] with interactions between C-C bonds is used. The time step is 0.5 fs for all calculations. To avoid any stretching or compressing stress on the GNR structure, free boundary conditions are applied to the y and z directions. The simulation domain is bounded with two Lennard-Jones (LJ) walls in the x direction that enclose all of the atoms. By applying LJ walls to the system, the GNR structure is fully relaxed during the thermal-equilibrium calculation and will not have a folding effect. The energy E of wall-particle interactions is given by the 9-3 LJ potential,

$$E = \varepsilon\left[\frac{2}{15}\left(\frac{\sigma}{r}\right)^9 - \left(\frac{\sigma}{r}\right)^3\right] r < r_c, \tag{7}$$

where r is the distance from the particle to the wall, and ε and σ are the usual LJ parameters, which are set to be 0.00284 eV and 3.4 Å, respectively. Also, r_c represents the cutoff distance specified in the simulation. The distance from each LJ wall to the GNR plane is set to be 0.335 nm, which is the distance between two neighboring carbon layers in the graphite structure. The configuration of the LJ walls is shown in Fig. 2.

Based on the PLTR technique, a numerical method is constructed to investigate the dynamic response of GNR and its thermophysical properties. In the MD simulation, a two-dimensional GNR with free boundary conditions is initially created. The GNR used in the MD simulation is of half length compared to that used in the PLTR experiment, since the MD simulation only applies the transient cooling process to one end of the GNR, while in experiment, both ends of the sample are maintained at RT. In the numerical method [Fig. 1(c)], the cooling area of the GNR stands for one of the sample-base contact points in the PLTR experiment, and the remaining part represents the half length of the sample that has been irradiated by a pulsed laser. For example, if the sample used in the PLTR experiment has a length of L, then only a $L/2$ GNR structure needs to be built in the simulation, which significantly reduces the computational time. The system is first heated to a higher temperature (325 K in our work) and reaches a thermal-equilibrium state before a cold impulse is added to one end of the GNR. The cooling

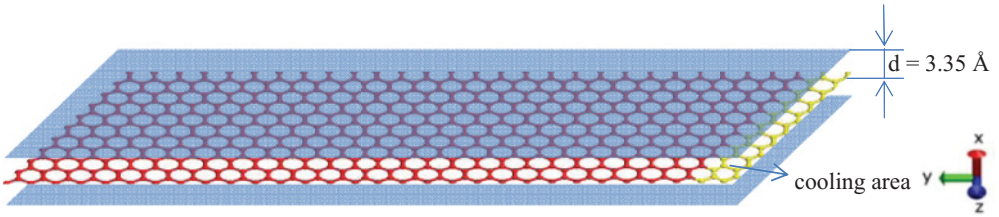

FIG. 2. (Color online) Structure of LJ walls in the x direction. The GNR is placed in the middle of the upper and lower LJ walls. The distance between the wall and the GNR plane is 3.35 Å.

area [shown in Fig. 1(c)] will maintain at a lower temperature (275 K), so the system will have thermal relaxation and reach thermal equilibrium again. To reach a steady state at 325 K before cooling relaxation starts, a canonical ensemble (NVT) condition is applied to the system for 500 ps. In the following 100 ps, a microcanonical ensemble (NVE) calculation is performed to assure the system's stability. After the thermal-equilibrium calculation, four layers of carbon atoms at one end of the GNR structure are chosen to form a "cooling group" whose temperature is "rescaled" to a value of 275 K and remains at this value through the relaxation process. The cooling procedure is accomplished by a velocity-rescaling approach. The "rescaling" process is only applied to the translational degrees of freedom for all atoms. This is an important consideration since extended spherical or aspherical particles, which have rotational degrees of freedom, may also reach an equilibrium state with this method. To assure the total momentum of the system is conserved during this rescaling process, a net velocity from the cooling group atoms is removed from the translational degrees of freedom before thermal rescaling takes place. The relaxation time used to reach a uniform temperature for the system is dependent on the length of the GNR and its thermal diffusivity. The data analysis method used in the PLTR technique could also be applied to this numerical approach. From the temperature-relaxation history, the thermal diffusivity of GNR can be calculated by global data fitting.

Compared with the NEMD and EMD approaches, this dynamic method takes much less time to measure the thermal diffusivity and has significantly reduced data uncertainty since more data points are used in the calculation (the average temperature of the whole system is used).

C. Quantum correction

In MD simulations, the temperature can be easily calculated from the time-average kinetic energy of atoms in the sample section within the simulation time using the energy equipartition theorem,

$$\langle E\rangle = \sum_{1}^{N} \frac{1}{2} m v_i^2 = \frac{3}{2} N k_B T_{MD}, \tag{8}$$

where $\langle E\rangle$ is the mean kinetic energy, v_i is the velocity of atoms, m is the atomic mass, N is the number of atoms in the system, and k_B is the Boltzmann constant.[26,27] However, it is worth pointing out that this method is valid only at high temperatures ($T \gg T_D$, where T_D is the Debye temperature). When the system temperature is lower than the Debye temperature, it is necessary to apply quantum correction to both the MD temperature and thermal-conductivity calculation. In the present work, we derived the quantum-correction equation for the two-dimensional GNR model as

$$T_{MD} = \frac{2}{3} T_{LA} x_{LA}^{-3} \int_0^{x_{LA}} \frac{x^2}{e^x - 1} dx + \frac{2}{3} T_{TA} x_{TA}^{-3} \int_0^{x_{TA}} \frac{x^2}{e^x - 1} dx + \frac{1}{3} T_{ZA} x_{ZA}^{-2} \int_0^{x_{ZA}} \frac{x}{e^x - 1} dx, \tag{9}$$

where T_{MD} is the temperature in the MD simulation; T_{LA}, T_{TA}, and T_{ZA} are the Debye temperatures of three different acoustic modes in GNR, which are 2840, 1775, and 1120 K respectively; and x_{LA}, x_{TA}, and x_{ZA} are the ratios of corrected temperatures (temperatures after quantum correction, denoted as T) and Debye temperatures. Given the values of T_{MD}, which are generated in the MD-simulation process, x_{LA}, x_{TA}, and x_{ZA} values can be determined by the inverse form of Eq. (9). In our work, first of all, a wide range of T values are substituted into Eq. (9) to get x_{LA}, x_{TA}, and x_{ZA}, and to calculate the corresponding T_{MD}. After we obtain the relations (a curve) between T_{MD} and T, the corrected temperatures can be calculated by interpolation based on a specified T_{MD}. The corresponding temperatures are then used to calculate the GNR's thermal conductivity and specific heat. Large differences between T_{MD} and T are observed in our work. For example, when T_{MD} decreases from 325 to 275 K in the MD simulation, corrected temperatures range from 725.8 to 658.8 K. It indicates that quantum correction is of great importance in the GNR's thermal-property calculation.

III. RESULTS AND DISCUSSION

To calculate GNR's thermal diffusivity, the initial and final temperatures of the system need to be provided. Therefore, NVE conditions are applied to the system both before and after cooling relaxation. The average temperature values in the two NVE calculations are then used as the upper and lower limits in global data fitting. During cooling relaxation, the temperature of the GNR's cooling area is kept at 275 K constantly, and the temperatures of the remaining part are recorded for each time step. Several millions of data sets will be recorded before the system reaches thermal equilibrium. The huge amount of temperature results not only makes it difficult for data analysis, but also induces significant noise into the results. To reduce the impact of this problem, the recorded temperature data are averaged each 100 time steps before global fitting, and also in the thermal-diffusivity and specific-heat calculations.

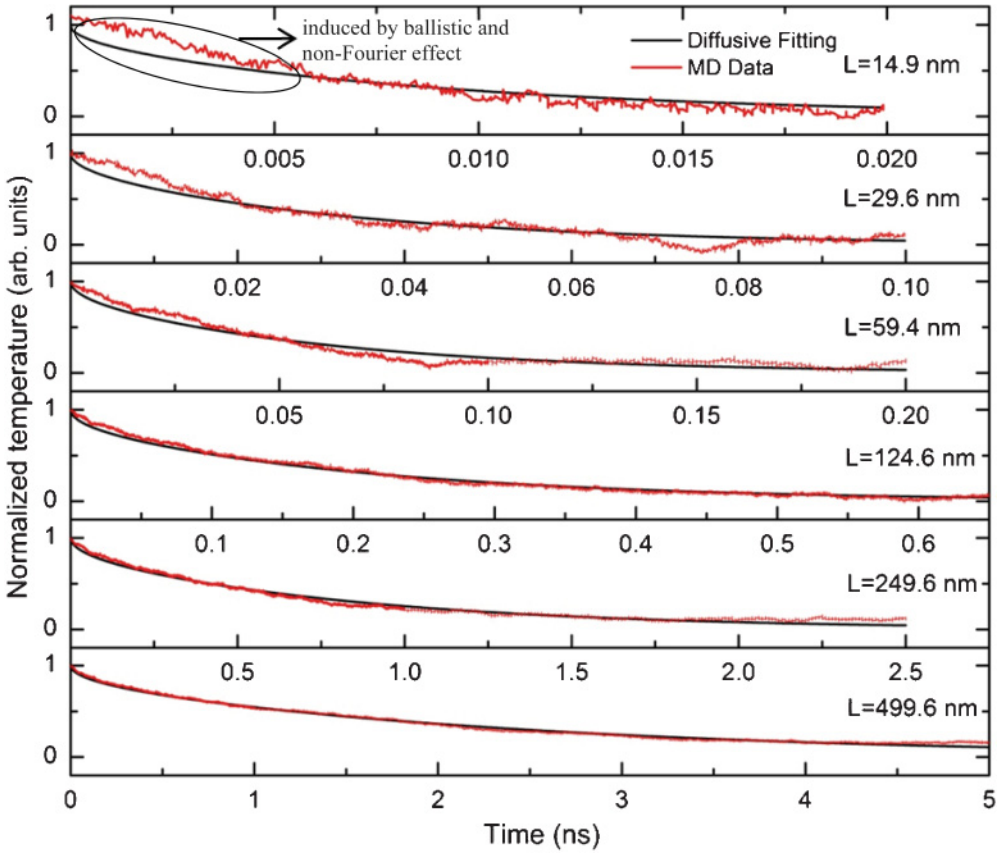

FIG. 3. (Color online) Global fitting results of different-length GNRs at 692.3 K. The lengths of the GNRs from top to bottom are 14.9, 29.6, 59.4, 124.6, 249.6, and 499.6 nm.

A. Fitting results of GNR and specific heat

In this work, GNRs of different lengths (14.9, 29.6, 59.4, 124.6, 249.6, 499.6, and 999.9 nm) are calculated for their thermal diffusivity. The thermal conductivities of all of the GNRs are calculated with the same MD parameters except the cooling-relaxation time. For 124.6-nm-long GNR as an example, after the system reaches thermal equilibrium at a temperature of 325 K, a cold impulse is applied, and it takes 650 ps for the cooling-relaxation process to finish. The quantum-corrected temperature results are then used in global data fitting to determine its thermal diffusivity, which is $2.9 \times 10^{-5} \mathrm{m}^2\ \mathrm{s}^{-1}$. After obtaining the thermal diffusivity, the thermal conductivity can be calculated by $k = \rho c_p \alpha$. The thermal conductivity is 95.8 $\mathrm{W\ m^{-1}\ K^{-1}}$ for 124.6-nm-long GNR. Figure 3 shows global fitting curves for GNRs of different lengths. As we can see from Fig. 3, with the length of the GNR increasing, the MD-simulation results will be more identical to theoretical results since more carbon atoms are used in the temperature calculation. Take a closer look at the fitting results in Fig. 3; it is found that the diffusive heat-transfer model has a lower temperature than the MD data at the beginning. Then, as time goes on, the agreement between them becomes better. Such an early-stage large difference could be induced by the non-Fourier-effect heat conduction and the ballistic effect of phonon thermal transport, which will be discussed later in this paper.

To obtain the dynamic thermal conductivity of GNR, graphene's specific heat needs to be calculated first. Since c_p values are the same for GNR structures around $T_{MD} = 300$ K, we choose the 59.4 nm GNR model for our study. After the 500 ps NVT and 50 ps NVE calculation, the system reaches a steady state at 295.5 K. Then, a heat flux of 3.3×10^7 $\mathrm{W\ m^{-2}}$ is added to the system continuously for 500 ps. After the heating process, the system reaches a steady state at 305.5 K. The temperature increase by this heating is 13.2 K after the quantum correction. The specific heat is calculated by $Q = c_p m \Delta T$, where Q is the total energy added to the system, m is the total mass of atoms, and ΔT is the temperature difference with the quantum correction. Q is expressed as $Q = q'' A t$, where A stands for the heating area and t stands for the heating time. The specific heat is calculated at 1.528×10^3 $\mathrm{J\ kg^{-1}\ K^{-1}}$ (at 692.3 K after quantum correction), which is nearly the same as graphite's specific heat of 1.519×10^3 $\mathrm{J\ kg^{-1}\ K^{-1}}$ (at 700 K).[28]

B. Thermal transport in GNRs

Ballistic transport has been observed when the phonon mean free path (MFP) is much larger than the size of the GNR that contains the medium through which the phonon travels, such that the phonon alters its motion only by hitting against the walls. Recent experiments suggest that thermal transport at the nanoscale is dominated by a ballistic rather than a diffusive

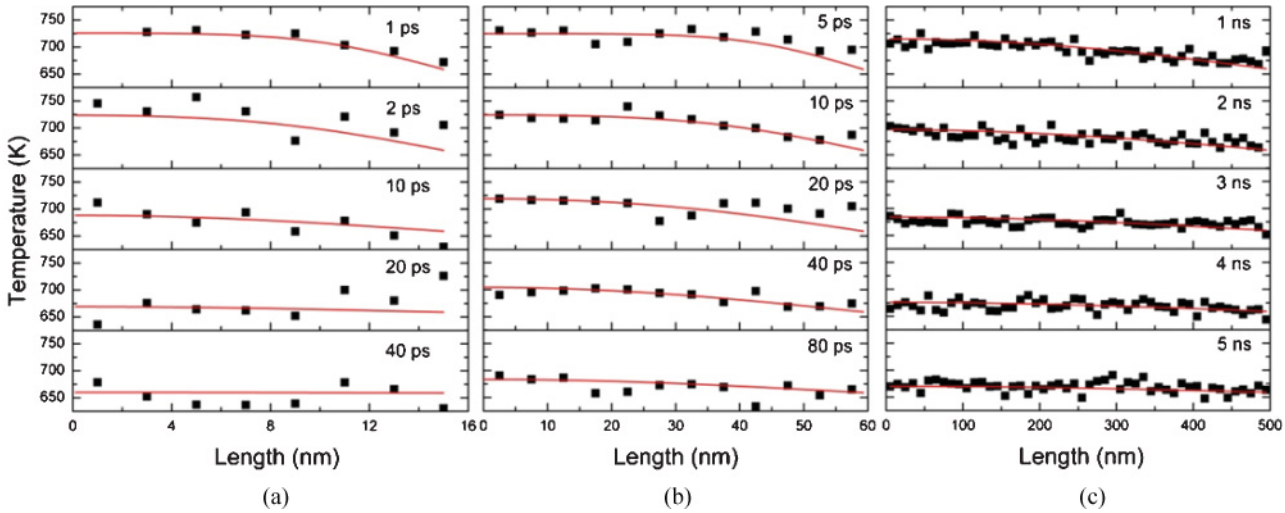

FIG. 4. (Color online) Spatial temperature evolution in GNRs at different times. The solid squares stand for the MD simulation results and the curves represent the theoretical results derived from the diffusive heat-conduction equation. The GNR length is 14.9, 59.4, and 499.6 nm for figures (a), (b), and (c), respectively.

mechanism.[12] The power-law relationship also implies that graphene conducts heat mainly through the ballistic transport mode in a low-temperature region.[29]

In this work, however, by comparing the spatial temperature distribution of GNR in the MD simulation with the theoretical results calculated from solving the diffusive heat-conduction equation, we could not see strong ballistic thermal transport in the GNR's in-plane direction. It is probably due to the statistical oscillation of the temperature that overshadows the ballistic thermal transport. Based on the diffusive mechanism along the in-plane direction of graphene, the transient heat-conduction equation $\partial T/\partial t = \alpha \cdot \partial^2 T/\partial x^2$ (α is thermal diffusivity) is solved by using the explicit method. Since the cooling-relaxation curve is dependent on the GNR's length and thermal diffusivity, to keep the consistency, initial and boundary conditions used in this calculation are identical to those in the MD simulations, including the α values. A short time step ($\Delta t = 10$ fs) and high spatial resolution ($\Delta x = 1$ nm) are employed in three different cases (14.9, 59.4, and 499.6 nm). The MD-simulation results agree well with the theoretical curves derived from the diffusive heat-conduction equation. It suggests that the thermal-transport mechanism in the GNR's in-plane direction is quite close to the diffusive situation. The temperature evolutions of the GNRs are shown in Fig. 4. Among the three GNR structures, the case for 14.9 nm requires the shortest time to reach the steady state, while the agreement is not as good as the other two due to the lack of sufficient temperature data points in space. The GNRs of 59.4 and 499.6 nm lengths show a sound agreement between the MD-simulation results and theoretical curves. This confirms the point that a longer sample length could give a more accurate evaluation of the thermal conductivity. Meanwhile, high accuracy for the values of thermal diffusivity derived from the PLTR physical model in the MD simulation is assured. Given the fact that the thermal transport inside the GNR could mainly be diffusive, Eq. (6), which is used for global fitting of the thermal diffusivity, is still within the diffusive limit. However, the ballistic effect is still important when the GNR length is small. From Fig. 3, it is shown that for short GNR structures, the beginning part of the MD-simulation results and fitting curves do not match as well as the longer ones, which are mainly induced by the ballistic effect (discussed in Sec. III D).

C. Size effect on thermal conductivity

To better compare our MD simulation results with previous experimental and numerical data, we also calculated GNRs' dynamic thermal conductivity and specific heat at 300.6 K (after quantum correction). During the cooling-relaxation process, the MD temperature decreases from 70 to 50 K, and a corresponding 324.8 to 276.6 K after quantum correction. For the 124.6 nm GNR as an example, its thermal diffusivity and thermal conductivity values are 4.1×10^{-5} m^2 s^{-1} and 72.6 W m^{-1} K^{-1}, respectively. The specific heat of the GNR at 300.6 K is calculated at 827 J kg^{-1} K^{-1}, which is close to graphite's value of 709 J kg^{-1} K^{-1} at the same temperature.[28] Although the thermal diffusivity of GNR is higher at 300.6 K than that at 692.3 K (2.9×10^{-5} m^2 s^{-1}), its thermal conductivity decreases due to a smaller specific heat. The calculated high values of the thermal conductivity suggest that the MFP in GNR is long, even at RT. The latter may result in a strong dependence of the thermal conductivity on the length l of the GNR and roughness of its edges, since the phonon boundary scattering starts to play a prominent role when l is comparable to the MFP. Therefore, the traditionally defined thermal conductivity is no longer an intrinsic property of materials. Instead, it changes with the length of materials. There are substantial experimental observations showing the thermal conductivity of thin films is significantly lower than that of bulk materials.[30–32] Figure 5 depicts GNR's thermal diffusivity and conductivity at different lengths. It can be concluded that the dynamic thermal conductivity of GNR increases with its length significantly.

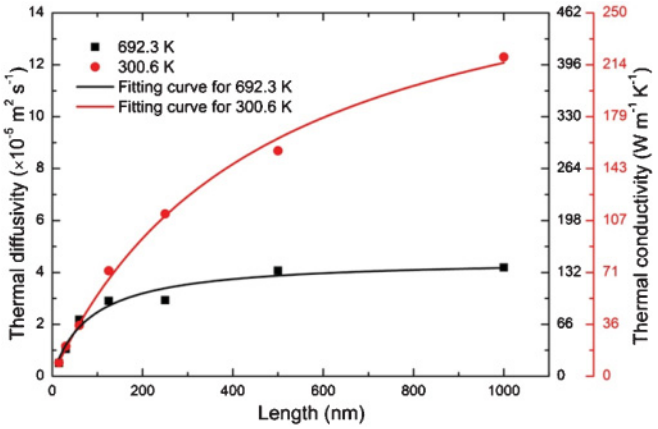

FIG. 5. (Color online) Thermal diffusivity (α) and thermal conductivity (k) variation against the GNR length.

For bulk materials, the kinetic theory gives the relationship between the macroscopic thermal conductivity and microscopic motions[33,34] as

$$k = \frac{1}{3}\rho c_p v l, \tag{10}$$

where k is the thermal conductivity, ρ is the mass density, c_p is the specific heat, v is the average phonon velocity, and l is the phonon mean free path, representing the average distance a phonon travels between successive collisions. In this sense, k is the one used in Fourier's law of heat conduction,

$$q'' = -k \cdot \nabla T, \tag{11}$$

where q'' is heat flux and T is temperature. Equation (10) is derived with the assumption that the space of particle motion is unbounded and is valid only if phonons can travel a very long distance before they hit the boundary. Equation (11) is simply a derivative of the more fundamental rule, the Boltzmann transport equation, under a steady state and quasi-equilibrium conditions.

Given the calculated thermal conductivity results for different GNRs at 692.3 and 300.6 K, we could derive k values for infinite-length GNRs using data fitting. Although it is no longer meaningful to refer to thermal conductivity as a basic physical concept at micro/nanoscales, its effective value is still of great importance from the engineering perspective and is expressed for a film structure as $k_{\text{eff}} = q''L/\Delta T$, where q'' is the heat flux at a steady state in the length direction, L is the film length, and ΔT is the temperature difference across the film. A material-independent relation is proposed as $k_{\text{eff}}/k = (1 + P \cdot l/L)^{-1}$, where k is the theoretical thermal conductivity of infinite-length GNR, l is the average phonon MFP, L is the length of the GNR sample, and P is the correlation related to boundary conditions and GNR shape. This equation is a universal relationship applicable in both ballistic and diffusive regimes of heat conduction. Since l is only related to internal scattering, its value for bulk materials can still be used and is calculated using the kinetic theory described by Eq. (10). It is worth noting that Eq. (10) is for three-dimensional situations and must be adapted as $k = \rho c_p v l/2$ for two-dimensional situations for GNR, in which the movement and scattering of phonons are confined in a plane. From the above equation, we can get the relationship between l and k for two-dimensional systems as $l = 2k/(\rho c_p v)$. Thus, k_{eff} could be expressed as

$$k_{\text{eff}} = \frac{k}{1 + 2P \cdot k/(\rho c_p v L)}. \tag{12}$$

To carry out this calculation, only phonon velocity v needs to be specified. According to Holland,[35] the following formula is a good approximation of the average phonon velocity within a wide temperature range:

$$\frac{1}{v} = \frac{1}{3}\left(\frac{1}{v_L} + \frac{2}{v_T}\right), \tag{13}$$

where v_L and v_T are the longitudinal and transverse sound speeds. Recent research by Nika *et al.*[14] indicates that the measured longitudinal and transverse velocities in graphene are $v_L = 21.3$ km s^{-1} and $v_T = 13.6$ km s^{-1}, respectively. Using Eq. (13), the calculated average phonon velocity for GNR is 15.5 km s^{-1}. Fitting the calculated thermal-conductivity values by using Eq. (12), P and k values are 14 and 149 W m^{-1} K^{-1}, respectively, at 692.3 K, while at 300.6 K, P and k are 20 and 317 W m^{-1} K^{-1}, respectively. The fitting results are shown in Fig. 5, and sound agreement is obtained between the fitting results and the MD data. Majumdar *et al.*[36] derived the relationship between k_{eff}/k and L/l as $k_{\text{eff}}/k = (1 + 4l/3L)^{-1}$ for a 2D heat-conduction situation. This equation is also based on the Boltzmann transport theory and indicates that P equals 4/3 for the diffusive-scattering boundary. Our calculated P values of 20 and 14 exceed the upper bound of diffusive scattering. Therefore, the thermal conductivity of GNR has been greatly reduced from the theoretical values and the reduction is not only attributed to boundary scattering, but also other changes induced by phonon frequency, phonon wave length, group velocity of phonons, and interactions among phonon branches.

As mentioned above, the quantum correction is of great significance in the calculation of GNR's thermal conductivity. Evans *et al.*[37] applied the EMD method to calculate the thermal conductivity of graphene ribbons with dimensions of 2×10 nm^2 at around 2000 W m^{-1} K^{-1}. The temperature they used is 300 K, which corresponds to 692.3 K after the quantum correction. From Eq. (1), we see that their calculated thermal conductivity would be more than five times smaller than their current results if quantum correction is applied. The non-Fourier effect is also observed at the beginning part of the GNR's thermal-relaxation process, which reduces the GNR's thermal conductivity to some extent. From the above discussion, we can conclude that our calculated thermal conductivity of GNR is within an acceptable range compared with previous studies.

D. Ballistic and non-Fourier effect in dynamic response

Most heat-conduction problems are described and analyzed using Fourier's law of heat conduction. However, it is well known that for transient problems in an extremely short period of time and very high heat flux, this classical diffusion theory may break down. The dynamic temperature responses under ultra-high-speed heating have shown some behavior that could not be predicted by the

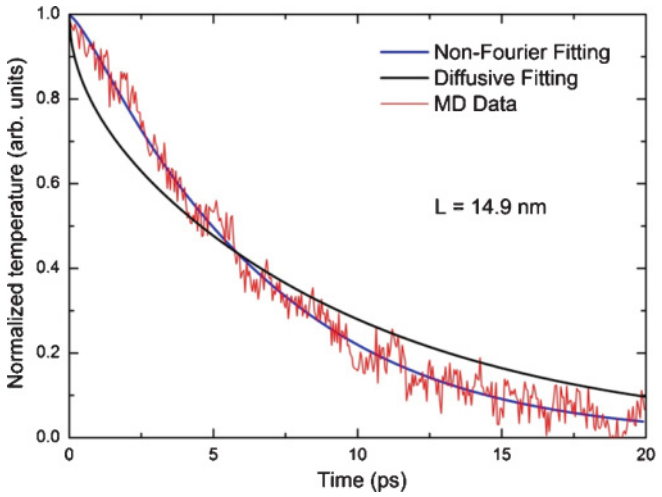

FIG. 6. (Color online) Comparison of non-Fourier fitting and diffusive fitting to the MD data. MD results are above the diffusive fitting curve in the first 6 ps due to a decreased effective thermal conductivity induced by the non-Fourier effect. The non-Fourier fitting curve matches the MD results soundly by using two relaxation times τ_q and τ_θ.

thermal-diffusion theory and many models have been developed to interpret these experiments.[38,39] Cattaneo and Vernotte formulated a well-known macroscopic description of thermal-wave propagation,[40,41] which is a conventional hyperbolic energy equation expressed as

$$\tau \frac{\partial^2 T}{\partial t^2} + \frac{\partial T}{\partial t} = \alpha \nabla^2 T, \tag{14}$$

where τ is the relaxation time of the thermal wave, and T and α are the temperature and thermal diffusivity, respectively. Joseph and Preziosi[38] described the microstructural effects by a relaxation function and decomposed it into two relaxation times, which lead to a description of a transient heat-conduction equation in the following generalized form:

$$\frac{1}{\alpha}\frac{\partial T}{\partial t} + \frac{\tau_q}{\alpha}\frac{\partial^2 T}{\partial t^2} = \nabla^2 T + \tau_\theta \frac{\partial}{\partial t}(\nabla^2 T). \tag{15}$$

For dielectric crystals, τ_q and τ_θ represent the relaxation times for momentum-nonconserving and momentum-conserving processes in the phonon system. A comparison of Eq. (15) with microscopic models suggests that if τ_q and τ_θ were formulated properly by some microscopic quantities, then this macroscopic model could fully describe the same heat-conduction equation as those in microscopic models. Cattaneo-Vernotte's thermal-wave law and Fourier's thermal-diffusion law are two special cases of this generalized model for $\tau_\theta = 0$ and $\tau_\theta = \tau_q = 0$.

In this work, four layers of carbon atoms at one end of the GNR are cooled to a low temperature in several time steps by a velocity-rescaling method. The use of this rapid cooling technique leads to an extremely high heat flux adjacent to the cooling area, and non-Fourier effects have been found to exist at the beginning part of the thermal-relaxation period (Fig. 3). To explore this non-Fourier mechanism, a numerical simulation based on the implicit finite-difference method is employed to study the temperature evolution of GNR and make a comparison with the MD result. One-dimensional discretization along the in-plane direction of the GNR with spacing $\Delta x = 1 \times 10^{-2}$ nm is conducted and a small time step with $\Delta t = 5 \times 10^{-2}$ ps is used. By fitting the MD results of 14.9 nm GNR using Eq. (15), we give the values of τ_q and τ_θ as 1.85 and 1.01 ps, respectively. The large value of τ_θ indicates that diffusive heat transfer is significant in GNR's thermal conductivity. The fitting curves are shown in Fig. 6. The thermal diffusivity of 14.9 nm GNR given

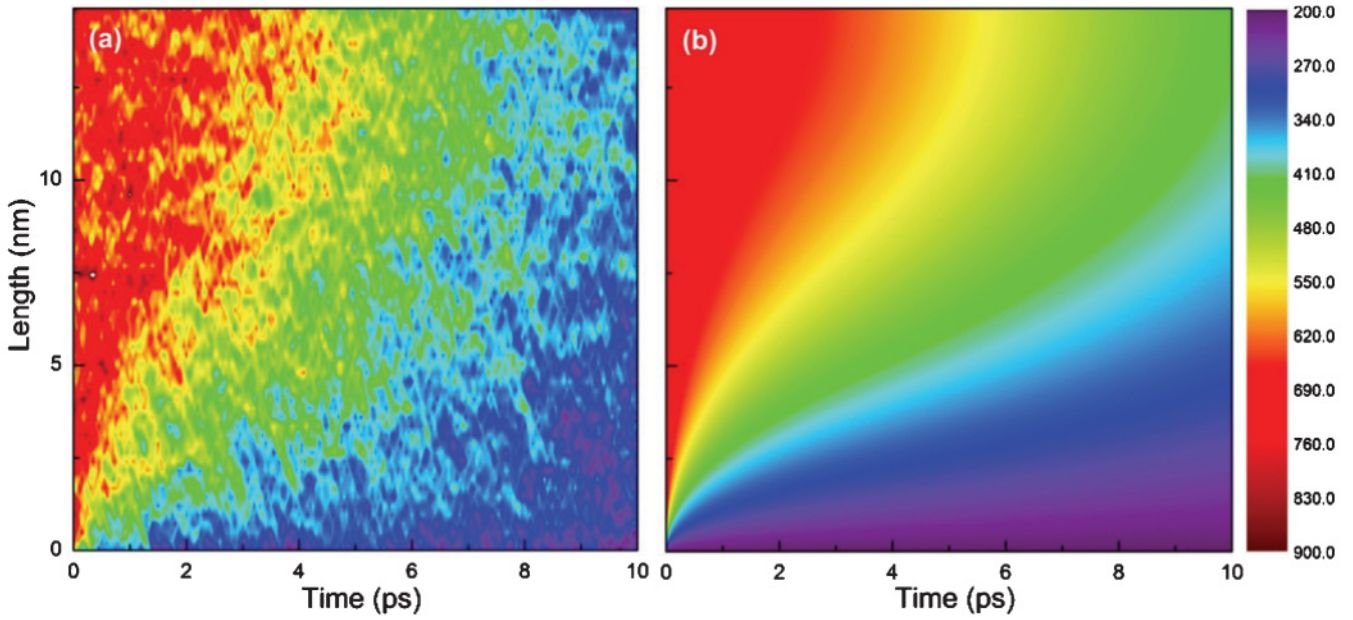

FIG. 7. (Color online) Spatiotemporal isotherms of 14.9 nm GNR with a cooling area located at the lower boundary. (a) MD results, and (b) numerical results calculated from the Fourier diffusive heat-conduction equation. The initial system temperature for both cases is 700 K, and then a cooling impulse of 200 K is added below the origin area.

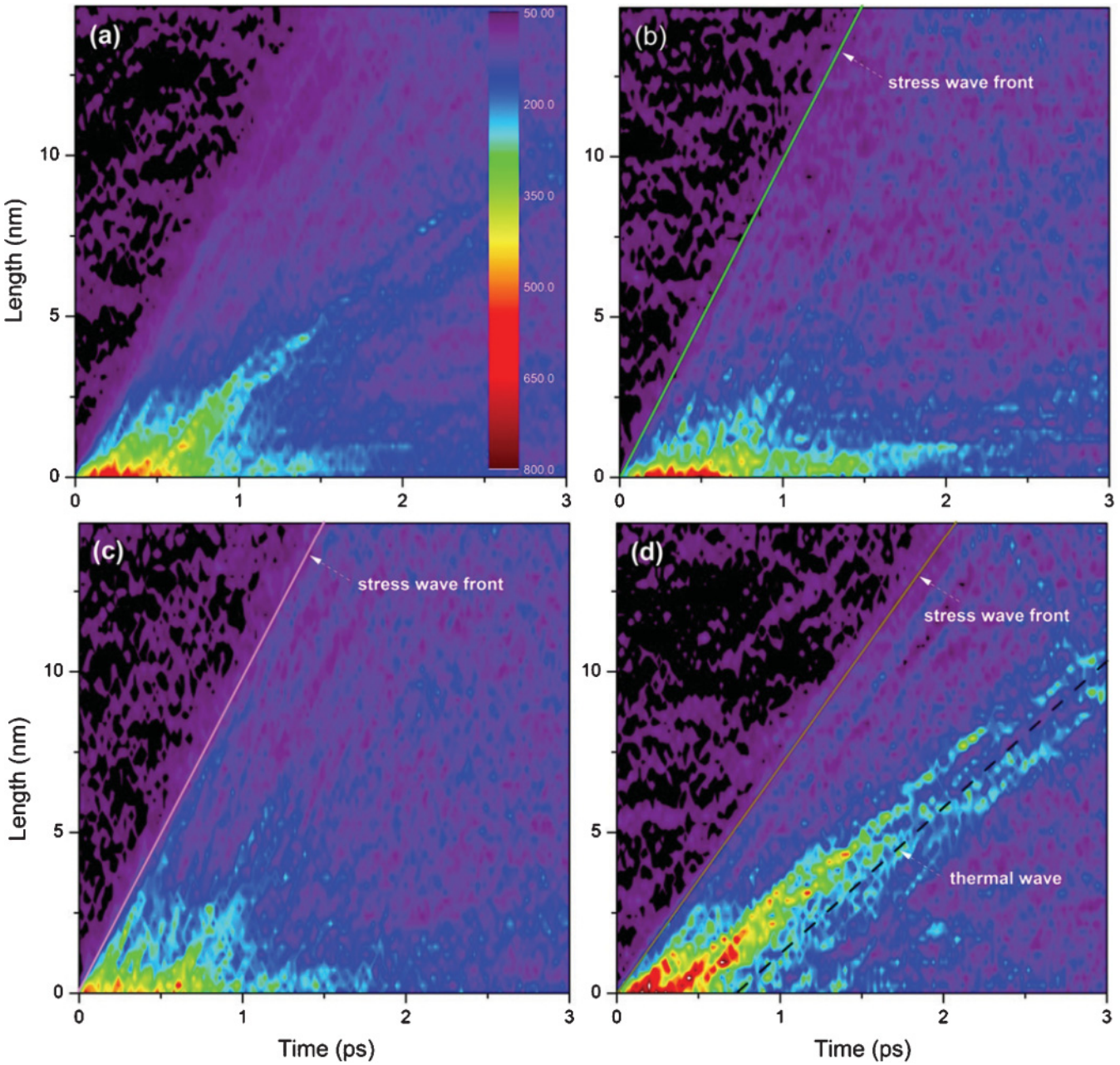

FIG. 8. (Color online) Spatiotemporal isotherms of 14.9 nm GNR with a thermal impulse imposed at the lower boundary for 0.4 ps: (a) overall temperature, (b) temperature of transverse phonons, (c) temperature of longitudinal phonons, and (d) temperature of flexural phonons. Solid lines represent the thermal-wave front.

by this fitting is 1.44×10^{-5} m^2 s^{-1}, which is larger than the value of 9.55×10^{-6} m^2 s^{-1} calculated by the previous pure diffusion model. Tang *et al.*[42] proved that a larger τ_θ will produce a higher rate of the thermal-diffusion effect and will result in a rapid temperature response in a short time. Since our calculated values of τ_q and τ_θ are in the same order, we could conclude that both diffusion conduction and thermal-wave conduction are affecting the GNR's thermal conductivity strongly at the beginning part. In Fig. 6, it could be seen that the MD temperatures decrease much slower than the diffusive fitting curve at the beginning, which could be explained by the thermal-wave effects in non-Fourier thermal conduction.

To better understand the effects induced by the ballistic thermal transport and non-Fourier heat conduction, we plot out the spatiotemporal isothermals of 14.9 nm GNR for both the MD results and numerical results that are calculated from Fourier's diffusive-heat equation. The results are shown in Fig. 7. As mentioned above, the GNR system has a cooling impulse of 275 K imposed on a 325 K thermal-equilibrium system to calculate the GNR's thermal diffusivity. However, the temperature difference (50 K) is very small compared with the data noise, which makes it difficult to justify the temperature change in isotherms. Therefore, we initially set the GNR system at 700 K to reach thermal equilibrium, and then a cooling impulse of 200 K is added to the cooling area.

For the full diffusion calculation, we use the thermal diffusivity at 300 K. The temperature of the cooling area, which is kept at 200 K, is not included in the contours. Figure 7(a) depicts the temperature evolution of the MD results from 700 to 200 K within the first 10 ps. Comparing the low-temperature areas (violet and blue regions) in Figs. 7(a) and 7(b), we notice that at the beginning of the heat conduction, the MD temperature diffuses slower than the numerical results, whereas after around 6 ps, the MD temperature diffuses faster than the numerical results. The temperature differences between the MD and numerical results can be explained by the non-Fourier effect. Figure 6 shows that the diffusive fitting curve decreases faster than the MD data at the beginning, and become flattened after around 6 ps. This is in sound agreement with the results shown in Fig. 7.

To take a further look at GNR's thermal-wave propagations, a thermal impulse is imposed upon one end of a 14.9 nm GNR. The system is initially kept at 50 K to reach thermal equilibrium. Then, four layers of carbon atoms at one end are connected to a Nose-Hoover thermostat kept at 1000 K for 0.4 ps. The remaining part of the GNR is divided into 64 unit cells along the length direction, with each containing about 20 atoms. The average energy of each unit cell is then used to calculate its temperature. The isotherm contours are shown in Fig. 8. The pictures depict how heat diffuses from the origin through the entire field. In the GNR system, heat is mainly transported by acoustic phonons, while the contribution from high-lying optic branches is small and negligible. Figures 8(b)–8(d) show the transverse (TA), longitudinal (LA), and flexural component of GNR's thermal-waves, respectively. Balandin *et al.*[43] calculated the lattice thermal conductivity of GNR and concluded that flexural acoustic phonons (ZA) do not make substantial contributions to heat conduction due to their low group velocity. However, recent experiments and theoretical analyses have proven that ZA phonons provide the dominant contribution to GNR's thermal conduction.[44–46] Seol *et al.*[47] carried out full quantum-mechanical calculations of the three-phonon scattering processes to obtain the phonon relaxation time for each phonon mode. They calculated the substrate-phonon scattering rate for the LA, TA, and ZA phonon modes and found that due to the large specific heat value of the ZA mode and large mean phonon-scattering time, the ZA mode contributed as high as 77% and 86% at 300 K and 100 K, respectively, for suspended GNR's thermal conductivity. By formulating the ballistic thermal conductance of phonons in a two-dimensional system and using the phonon's dispersion relation, Nakamura *et al.*[48] calculated the contributions of the LA, TA, and ZA phonons to graphene's thermal conductance. They concluded that the ballistic phonon conductance is determined by the ZA phonon modes below about 20 K, and that contributions of the TA and LA phonon modes cannot be neglected above 20 K, while the ZA phonon modes are still dominant. Although much work has been done to analyze the ZA mode's effect on GNR's thermal conductivity, to our best knowledge, there are no MD simulations that have been done to prove this valuable theorem. In the present work, we can clearly see in Fig. 8(d) that a strong thermal-wave propagates through the spatiotemporal isotherms (ZA mode), while in Figs. 8(b) and 8(c), no evident thermal waves are observed. When the thermal-relaxation time of phonons is large, the thermal-wave effect will be more prominent. Therefore, we conclude that the ZA mode is more significant than the LA and TA modes in respect to GNR's thermal conductivity. Also we can conclude that during thermal transport by the ZA phonons, the energy transfer among ZA phonons is much faster than that between ZA and LA/TA phonons. This is because if the ZA↔LA/TA phonon energy exchange were comparable to the ZA↔ZA energy exchange, then the thermal wave could also be observed in the LA and TA temperature evolution. However, no thermal wave is observed in the spatiotemporal isotherms of LA and TA phonon temperatures.

In these spatiotemporal isotherms, group velocities for the TA, LA, and ZA mode are identified. When the 1000 K thermal impulse is imposed on one end of the GNR, a local stress will be generated and will propagate in the in-plane directions. The local temperatures of the GNR will remain unchanged until this stress wave arrives and its propagation speed can be measured, as shown in Fig. 8. Stress-wave fronts are denoted by solid lines in Fig. 8. Since these velocities represent the energy transmission speed in the GNR, they are also known as group velocities (v_g). From Fig. 8, the group velocities of the TA, LA, and ZA modes are calculated at 9.8, 9.8, and 7.0 km s^{-1} respectively. Group velocities could be calculated from GNR's dispersion relation by the expression $v_g = d\omega/dk$, where ω is the angular frequency and k is the wave number. Wirtz *et al.*[49] compared GNR's phonon-dispersion relations calculated by Dubay *et al.*[50] and Maultzsch *et al.*[51] The result is shown in Fig. 9. From the TA, LA, and ZA dispersion relation curves in Fig. 9, different group velocities for each phonon branch can be calculated. On the TA curve from the GNR's dispersion relation, the average group velocities calculated in the AB and DF regions are 9.7 and 9.8 km s^{-1}, respectively. For the LA mode, the EF region contributes to the group velocity measured in Fig. 8(c) and the average group velocity in this region is 9.7 km s^{-1}. For the ZA mode, regions AC and FG have average group velocities at 6.8 and

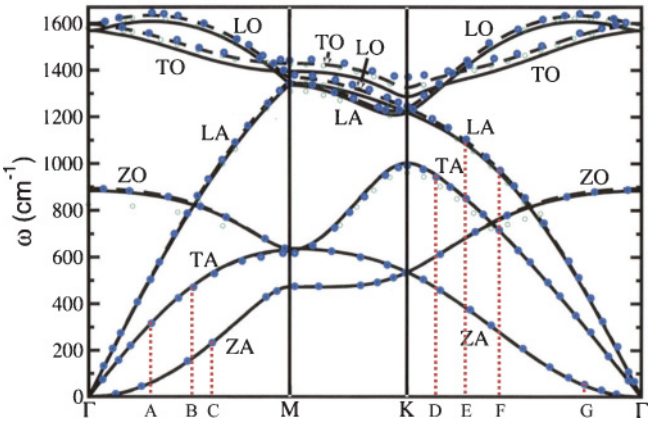

FIG. 9. (Color online) Phonon-dispersion relations of graphene based on *ab initio* calculation.[49] The three-phonon dispersion branches, which originate from the Γ point of the first Brillouin zone, correspond to acoustic modes and the remaining three branches are for optical modes. The regions that correspond to different group velocities in Fig. 8 are denoted by dashed lines (with permission from Elsevier for use in this paper).[49]

7.0 km s^{-1} and contribute to the group velocity in Fig. 8(d). A theoretical study of the second sound wave under the linear approximation for three-dimensional materials shows that thermal-wave-propagation velocity is $c = v_g/\sqrt{3}$,[52] where v_g is the group velocity. For two-dimensional GNR, this relation should be modified as $c = v_g/\sqrt{2}$.[53] In Fig. 8(d), the thermal-wave-propagation velocity is calculated at 4.6 km s^{-1} for the ZA mode, as denoted by the dashed line in Fig. 8(d). Based on the group velocity in Fig. 8(d), the thermal-wave speed is predicted at $c = v_g/\sqrt{2} = 7.0/\sqrt{2} = 4.9$ km s^{-1}. This value agrees well with the thermal-wave speed of 4.6 km s^{-1} observed in Fig. 8(d).

IV. CONCLUSION

A fast transient technique was developed to characterize the thermophysical properties of GNRs using an MD simulation. A Debye model for two-dimensional GNR was derived for the temperature's quantum correction. The specific heat of GNRs was calculated using an MD simulation and the results are 1528 and 827 J kg^{-1} K^{-1} at 692.3 K and 300.6 K, respectively. These values are very close to those of graphite, and suggest that the unique 2D structure of graphene has little effect on its ability to store thermal energy. Based on obtained thermal-conductivity data at different lengths, the thermal conductivity for infinite-length GNRs was calculated at 149 W m^{-1} K^{-1} (692.3 K) and 317 W m^{-1} K^{-1} (300.6 K). These values are much smaller than some data reported in the literature for GNRs of similar width. It reflects the fact that the quantum correction of the temperature is critical for the thermal-transport study of graphene. The calculated thermal conductivity is reduced by boundary scattering and other property changes due to the restriction of small width (1.99 nm). Non-Fourier heat conduction was observed to be significant in 14.9-nm-long GNR, and a wavelike heat flux is observed in the transient heating of a GNR system. A thermal wave was only observed for the ZA phonon, suggesting that thermal transport by ZA phonons is faster than that by the TA and LA modes. It is conclusive that the ZA mode is dominant for GNR's thermal conduction. Also, the energy transfer among ZA phonons is much faster than that between ZA and LA/TA phonons. The observed propagation speed ($c = 4.6$ km s^{-1}) of the thermal wave follows the relation of $c = v_g/\sqrt{2}$, where v_g is the ZA phonon group velocity (7.0 km s^{-1} from our calculation).

ACKNOWLEDGMENTS

This work was partially supported by the U.S. Army Research Office under Contract No. W911NF1010381. Also, partial support of this work from the National Science Foundation (Grants No. CBET-0931290, No. CMMI-1029072, No. CBET-0932573, and No. CMMI-0926704) is gratefully acknowledged.

*xwang3@iastate.edu.

[1] A. K. Geim and K. S. Novoselov, Nature Mater. **6**, 183 (2007).
[2] Y. W. Son, M. L. Cohen, and S. G. Louie, Nature (London) **444**, 347 (2006).
[3] K. S. Novoselov, A. K. Geim, S. V. Morozov, D. Jiang, Y. Zhang, S. V. Dubonos, I. V. Grigorieva, and A. A. Firsov, Science **306**, 666 (2004).
[4] J. S. Bunch, A. M. van der Zande, S. S. Verbridge, I. W. Frank, D. M. Tanenbaum, J. M. Parpia, H. G. Craighead, and P. L. McEuen, Science **315**, 490 (2007).
[5] Y. Yue, J. Zhang, and X. Wang, Small (unpublished).
[6] T. Kawai, M. Hino, T. Ebisawa, S. Tasaki, D. Yamazaki, Y. Otake, G. Shirouzu, and N. Achiwa, Physica B **276**, 977 (2000).
[7] A. Rycerz, J. Tworzydlo, and C. W. J. Beenakker, Nature Phys. **3**, 172 (2007).
[8] K. Wakabayashi, Y. Takane, and M. Sigrist, Phys. Rev. Lett. **99**, 036601 (2007).
[9] T. Yamamoto, S. Watanabe, and K. Watanabe, Phys. Rev. Lett. **92**, 075502 (2004).
[10] Z. X. Guo, D. Zhang, and X. G. Gong, Appl. Phys. Lett. **95**, 163103 (2009).
[11] A. A. Balandin, S. Ghosh, W. Z. Bao, I. Calizo, D. Teweldebrhan, F. Miao, and C. N. Lau, Nano Lett. **8**, 902 (2008).
[12] S. Ghosh, I. Calizo, D. Teweldebrhan, E. P. Pokatilov, D. L. Nika, A. A. Balandin, W. Bao, F. Miao, and C. N. Lau, Appl. Phys. Lett. **92**, 151911 (2008).
[13] T. Ouyang, Y. P. Chen, K. K. Yang, and J. X. Zhong, Europhys. Lett. **88**, 28002 (2009).
[14] D. L. Nika, E. P. Pokatilov, A. S. Askerov, and A. A. Balandin, Phys. Rev. B **79**, 155413 (2009).
[15] B. D. Kong, S. Paul, M. B. Nardelli, and K. W. Kim, Phys. Rev. B **80**, 033406 (2009).
[16] J. N. Hu, X. L. Ruan, and Y. P. Chen, Nano Lett. **9**, 2730 (2009).
[17] N. Mingo and D. A. Broido, Phys. Rev. Lett. **95**, 096105 (2005).
[18] Y. Xu, X. B. Chen, B. L. Gu, and W. H. Duan, Appl. Phys. Lett. **95**, 233116 (2009).
[19] D. W. Brenner, O. A. Shenderova, J. A. Harrison, S. J. Stuart, B. Ni, and S. B. Sinnott, J. Phys. Condens. Matter **14**, 783 (2002).
[20] P. K. Schelling, S. R. Phillpot, and P. Keblinski, Phys. Rev. B **65**, 144306 (2002).
[21] S. Berber, Y. K. Kwon, and D. Tomanek, Phys. Rev. Lett. **84**, 4613 (2000).
[22] J. Q. Guo, X. W. Wang, D. B. Geohegan, and G. Eres, Funct. Mater. Lett. **1**, 71 (2008).
[23] J. Q. Guo, X. W. Wang, D. B. Geohegan, G. Eres, and C. Vincent, J. Appl. Phys. **103**, 113505 (2008).
[24] B. W. Dodson, Phys. Rev. B **35**, 2795 (1987).
[25] J. Tersoff, Phys. Rev. Lett. **61**, 2879 (1988).
[26] N. Yang, G. Zhang, and B. W. Li, Nano Lett. **8**, 276 (2008).
[27] X. P. Huang, X. L. Huai, S. Q. Liang, and X. W. Wang, J. Phys. D **42**, 095416 (2009).
[28] Frank P. Incropera and David P. Dewitt, *Fundamentals of Heat and Mass Transfer* (Wiley, Hoboken, NJ, 2007).
[29] E. Munoz, J. X. Lu, and B. I. Yakobson, Nano Lett. **10**, 1652 (2010).

[30]J. C. Lambropoulos, M. R. Jolly, C. A. Amsden, S. E. Gilman, M. J. Sinicropi, D. Diakomihalis, and S. D. Jacobs, J. Appl. Phys. **66**, 4230 (1989).
[31]S. R. Mirmira and L. S. Fletcher, J. Thermophys. Heat Transfer **12**, 121 (1998).
[32]D. G. Cahill, Microscale Therm. Eng. **1**, 85 (1997).
[33]J. M. Ziman, Philos. Mag. **5**, 757 (1960).
[34]S. Volz, J. B. Saulnier, M. Lallemand, B. Perrin, P. Depondt, and M. Mareschal, Phys. Rev. B **54**, 340 (1996).
[35]M. G. Holland, Phys. Rev. **132**, 2461 (1963).
[36]A. Majumdar, Trans. ASME: J. Heat Transfer **115**, 7 (1993).
[37]W. Evans, Appl. Phys. Lett. **96**, 203112 (2010).
[38]D. D. Joseph and L. Preziosi, Rev. Mod. Phys. **61**, 41 (1989).
[39]M. N. Ozisik and D. Y. Tzou, Trans. ASME: J. Heat Transfer **116**, 526 (1994).
[40]P. Vernotte, C.R. Acad. Sci. **246**, 3154 (1958).
[41]C. Cattaneo, C.R. Acad. Sci. **247**, 431 (1958).
[42]D. W. Tang and N. Araki, Mater. Sci. Eng. A **292**, 173 (2000).
[43]A. A. Balandin, D. L. Nika, S. Ghosh, and E. P. Pokatilov, Appl. Phys. Lett. **94**, 203103 (2009).
[44]L. Lindsay, D. A. Broido, and N. Mingo, Phys. Rev. B **83**, 235428 (2011).
[45]L. Lindsay, D. A. Broido, and N. Mingo, Phys. Rev. B **82**, 115427 (2010).
[46]B. W. Li, Z. Q. Wang, R. G. Xie, C. T. Bui, D. Liu, X. X. Ni, and J. T. L. Thong, Nano Lett. **11**, 113 (2011).
[47]L. Shi *et al.*, Science **328**, 213 (2010).
[48]K. Saito, J. Nakamura, and A. Natori, Phys. Rev. B **76**, 115409 (2007).
[49]L. Wirtz and A. Rubio, Solid State Commun. **131**, 141 (2004).
[50]O. Dubay and G. Kresse, Phys. Rev. B **67**, 035401 (2003).
[51]J. Maultzsch, S. Reich, C. Thomsen, H. Requardt, and P. Ordejon, Phys. Rev. Lett. **92**, 075501 (2004).
[52]M. Chester, Phys. Rev. **131**, 2013 (1963).
[53]X. Xu and X. Wang, Appl. Phys. A **73**, 107 (2001).